Korean J. Chem. Eng., 34(8), 2311-2324 (2017)
DOI: 10.1007/s11814-017-0086-1

pISSN: 0256-1115
eISSN: 1975-7220

Decreasing ICP of forward osmosis (TFN-FO) membrane through modifying PES-Fe_3O_4 nanocomposite substrate

Rezvaneh Ramezani Darabi, Majid Peyravi, Mohsen Jahanshahi†, and Ali Asghar Qhoreyshi Amiri

Nanotechnology Institute, Faculty of Chemical Engineering, Babol Noshirvani University of Technology, Babol, Iran
(*Received 24 November 2016 • accepted 20 March 2017*)

Abstract−This film nanocomposite forward osmosis (TFN-FO) membrane was developed using polyethersulfone-ferrous ferric oxide (PES-Fe_3O_4) nanocomposite substrate. The results revealed that the porosity and the hydrophilicity of the PES substrate were improved after addition of Fe_3O_4 nanoparticles (NPs), leading to reducing in structural parameter (*S* value or *S*) and water flux enhancement. To fabricate TFN membranes for FO application, a thin polyamide layer was fabricated by interfacial polymerization of m-Phenylenediamine (MPD) and 1, 3, 5-trimesoylchloride (TMC) on the top surface of PES-Fe_3O_4 nanocomposite substrates. The TFN membrane prepared with 0.2 wt% Fe_3O_4 NPs showing the most reliable results by exhibiting high water flux and low reverse solute flux. Furthermore, TFN0.2 membrane exhibited significantly higher pure water flux than that of control thin film composite (TFC) membrane in both AL-FS and AL-DS orientation when 10 mM NaCl and Caspian seawater was used as feed solution and 0.5 or 2 M NaCl was used as draw solution. This improvement can be attributed to the fact that the *S* value of TFN0.2 is much lower in comparison to control TFC membrane (0.42 vs 0.78 mm), leading to reduced internal concentration polarization (ICP) effect.

Keywords: Internal Concentration Polarization, Fe_3O_4 Nanoparticle, Thin Film Nanocomposite Substrate, Forward Osmosis

INTRODUCTION

Due to dry climate and shortage of water resources in Iran, the Caspian Sea (a large saltwater lake located between Europe and Asia) has been considered as a potential resource for the production of desalinated potable and agricultural water for Iran. Thus, appropriate desalination technology with higher water flux and higher recovery should be regarded [1].

Forward osmosis (FO) process has been identified as an emerging technology because of its unique features such as low energy consumption, no or low hydraulic pressure, high water recovery and more extensive applications such as seawater desalination, protein and pharmaceutical enrichment, food processing, power generation and biological process. The FO process relies on using the osmotic process to draw the water across a permeable membrane from a feed water to a higher concentrated solution (draw solution). The driving force is hence created naturally by the difference in osmotic pressure (i.e., the chemical potential difference) between the draw solution and the feed solution [2-9]. However, there are some obstacles to be overcome. One e challenging issue in FO is concentration polarization (CP). Both external CP (ECP) and internal CP (ICP) can take place in FO processes. ECP occurs at the active layer (AL) of the FO membrane and ICP occurs in the support layer of the FO membrane. However, the negative effect of ECP on the pure water flux can be mitigated by increasing the velocity or flow turbulence. ICP generates large boundary layer within the substrate and could decrease the water flux by more than 80% [10-15]. It is generally well known that small structural parameter, *S* (*S*=thickness×tortuosity/porosity) is preferable for a support layer (sublayer) to minimize the ICP effect during FO process. The smaller *S* value can be achieved by constructing higher porosity, lower tortuosity and thinner structure of support layer [11,16]. Membrane support chemistry, most remarkably hydrophilicity, may also play a significant role in the severity of ICP [17].

Some literature has mainly focused on finding an effective way to mitigate the ICP phenomena during FO process. Yasukawa et al. used polyketone membranes as a novel substrate for the preparation of high-performance FO membranes. This TFC FO membrane improved FO efficiency because of its highly porous structure and large pore size that dramatically reduced the parameters of the polyketone membrane structure [18]. Puguan et al. synthesized crosslinked polyvinyl alcohol (PVA) nanofibers membrane as a porous support layer for the fabrication of TFC FO membranes. The fabricated TFC membrane improved FO efficiency because of its low *S* value and remarkable hydrophilic property [19].

In recent years, mixed-matrix membranes embedded by inorganic nanoparticles such as zeolite, TiO_2 [20,21] and SiO_2 [22] have attracted a great deal of attention. The literature has shown that the incorporation of nanoparticles into the polymeric matrix not only improves the structure and physicochemical properties (porosity, hydrophilicity, mechanical stability and pore size) of polymeric membranes, but also demonstrates unique functionalities such as photocatalytic and antibacterial characteristics for the polymeric membranes. This concept was mainly used to mitigate ICP, which has negatively impacted the PRO and FO processes because it can significantly decrease the osmotic driving force and therefore lower the water flux [23-25].

Tian et al. incorporated different amounts of SiO_2 nanoparticles

†To whom correspondence should be addressed.
E-mail: mmohse@yahoo.com

Table 1. The composition of casting solution and monomer solutions used for the TFC/TFN FO membrane preparation

FO membrane	Composition of casting solution				Composition of aqueous and organic solution for PA layer formation	
	PES (wt%)	PVP (wt%)	DMF (wt%)	Fe_3O_4 (wt%)	MPD/water (wt/v%)	TMC/n-hexane (wt/v%)
TFC (control)	14	2	84.00	0	2	0.1
TFN0.06	14	2	83.94	0.06	2	0.1
TFN0.1	14	2	83.90	0.1	2	0.1
TFN0.2	14	2	83.80	0.2	2	0.1
TFN0.3	14	2	83.70	0.3	2	0.1
TFN0.4	14	2	83.60	0.4	2	0.1
TFN0.5	14	2	83.50	0.5	2	0.1

in the nanofibrous substrate for the synthesis of FO membranes to mitigate undesired ICP. It improved the FO water flux, which was attributed to the high porosity of the membrane and large pore sizes that dramatically reduced the parameters of the membrane structure [22] Ghanbari et al. were able to control the ICP by adding halloysite nanotubes into the substrate. The low structural parameter of TFN membranes can be explained by the fact that the addition of halloysite nanotubes enhances the hydrophilicity and increases the porosity and pore sizes of the substructure [26]. Lu et al. fabricated a novel TFN FO membrane based on a layered double hydroxide (LDH) nanoparticle blended ultrafiltration substrate. The addition of LDH nanoparticles endowed the ultrafiltration substrate with increased surface hydrophilicity, porosity and surface pore diameter. Consequently, all resultant TFN FO membranes decreased *S* value and increased water flux as compared with TFC FO membrane [27]. Kuang et al. successfully incorporated calcium carbonate ($CaCO_3$) nanoparticles into mixed matrix PSF FO membrane fabrication. The results demonstrated that the substrate TFC membranes fabricated with $CaCO_3$ nanoparticles exhibited higher porosity and smaller *S* value, which is beneficial for improving water flux and reducing mass transfer resistance [28].

Compared with other nanomaterials, ferrous ferric oxide (Fe_3O_4) nanoparticle was used as inorganic nanofiller additive in membrane fabrication due to its numerous advantages, such as low toxicity, good biocompatibility, high surface area, chemical stability and special magnetic properties [29-33].

In this study, we have attempted to fabricate novel TFN membranes which are suitable for FO process by modifying the PES substrate properties using hydrophilic Fe_3O_4 nanoparticles. Influence of Fe_3O_4 incorporation on the main properties of the substrate with respect to hydrophilicity, porosity, pore size, cross-sectional morphology, roughness, and water flux was systematically investigated. Implications of nanomaterials are discussed to specify how the incorporation of Fe_3O_4 can influence ICP, *S* value, water flux and salt rejection of TFN FO membranes. To the best of our knowledge, this is the first study on TFN membrane using PES-Fe_3O_4 nanocomposite substrate for FO applications.

EXPERIMENTAL

1. Materials

Polyethersulfone (PES, ultrason 6020) was used for preparing the membrane substrates. N, N-dimethylformamide (DMF, >99.8%, Merck) was used as the solvent for providing the casting solution. Polyvinyl pyrrolidone (PVP, Merck) was used as an additive and pore former in the casting solution. Ferrous ferric oxide (Fe_3O_4, 99.5%, 20-30 nm, USNANO) was added to the polymeric dope solution to improve substrate properties. Also, sodium dodecyl sulfate (SDS, Merck) was used. Materials used for interfacial polymerization included m-Phenylenediamine (MPD, >95%, Merck), n-hexane (>95%, Merck) and 1,3,5-trimesoylchloride (TMC, >98%, Merck). Sodium chloride (NaCl, >99%, Dr. Mojallali) solution was used for both FO and RO experiments.

2. Synthesis of Flat-sheet TFN FO Membranes

2-1. Preparation of FO Support Layer

Table 1 presents the characteristics of five substrates prepared in this study using PES-based dope solutions. To make a dope solution, an appropriate amount of Fe_3O_4 nanoparticles and PVP was first added to DMF, followed by 30 min ultrasonication to minimize Fe_3O_4 agglomeration. In the following step, PES was added to the solution under fast stirring. The dope solution was then degassed at 25 °C for 5 h to remove the trapped air bubbles. The polyester non-woven fabric was attached to a glass plate and then the dope solution was cast on a polyester using casting knife at a thickness of 100 μm. After that, the glass plate was immersed smoothly in a precipitation bath including 2 wt% DMF and 0.1% wt/v SDS in DI water at room temperature to initiate the phase inversion. After 30 min, the resulting PES substrate was immersed in a water bath for one day to remove the excess solvent and additive. As the final stage, the PES membrane was dried via placing between two sheets of filter paper for one day at room temperature.

2-2. Preparation of Polyamide Rejection Layer

The active layer of TFN membrane was formed on the surface of the PES substrate by interfacial polymerization between MPD and TMC. The membrane sublayer was first immersed in a 2 wt% MPD solution for 2 min. After removing the excess MPD solution by rubber roller, the MPD saturated PES support layer was soaked in a 0.1 wt% of TMC dissolved in n-hexane for 30 s. The resultant TFC membrane was dried at 80 °C for 5 min in an oven for post treatment and then was kept in deionized water at room temperature for characterization.

3. Evaluation of Membrane Performance

The water permeability and selectivity of the TFN membranes were tested using a cross-flow RO experimental. The effective sur-

face area of the membrane was 38 cm^2 inside the permeation cell. RO experiments used feed solution containing 20 mM NaCl at 2.5 bar. Pure water flux (J) and water permeability (A) [21] of the membranes were calculated using Eqs. (1) and (2) as follows:

$$J = \frac{\Delta V}{A_m \cdot \Delta t} \quad (1)$$

$$A = \frac{J}{\Delta P} \quad (2)$$

where A_m is effective membrane area, and ΔV is permeate volume, Δt is time and ΔP is pressure difference. To evaluate membrane salt rejection rate R, the following equation is employed:

$$R = \left(1 - \frac{C_p}{C_f}\right) \times 100 \quad (3)$$

In this equation, C_f and C_p represent salt concentrations in the feed and permeate solution, respectively. The salt permeability coefficient (B) [34] of membrane was determined based on solution-diffusion theory by:

$$\frac{1-R}{R} = \frac{B}{A(\Delta P - \Delta \pi)} \quad (4)$$

where A is pure water permeability, ΔP is pressure difference and $\Delta \pi$ is the osmotic pressure gradient across the membrane. The FO performance of the TFN membrane such as water flux and salt permeability was determined in a lab-scale FO setup. Both feed and draw solutions were circulated at a constant velocity of 800 mL/min. Also, the temperature of feed and draw solutions was constant at room temperature during the FO test. A digital weight balance was placed at the bottom of the draw solution tank to measure the water flux of FO membranes. Solution conductivity was determined with a conductivity meter (Model: WA-2017SD, Taiwan) and was consequently converted into concentration using a calibration curve. All the TFN membranes were tested under two different orientations: FO mode (support layer facing the draw solution (AL-FS)) and pressure retarded osmosis (PRO) mode (support layer facing the feed solution (AL-DS)). Each experiment was run for 30 min and was repeated three times to obtain an average data. In the FO system, 10 mM and Caspian Sea solutions were used as the feed and different concentrations of aqueous NaCl solution (0.5 and 2.0 M) were used as the draw solution. The FO membrane water flux J_v was determined by measuring the weight change of draw solution [35]:

$$J_v = \frac{\Delta V}{A_m \cdot \Delta t} = \frac{\Delta m/\rho}{A_m \cdot \Delta t} \quad (5)$$

where ΔV and Δm are the volume and weight changes of the draw solution, respectively. ρ is the density of feed solution, A_m is effective membrane area and Δt is the measuring time interval. The FO solute flux J_s was determined from the salt concentration in the feed solution after 30 min operation by the following equation [36].

$$J_s = \frac{V_t C_t - V_0 C_0}{A_m \cdot \Delta t} \quad (6)$$

where V_0 and V_t are the initial and final volumes of the feed, and C_0 and C_t are the salt concentration of feed solution measured at the beginning and the end of the FO test. According to the classical ICP model developed by Loeb et al. [35], the water flux of FO membranes was obtained experimentally from the following equations for dilutive ICP (AL-FS) and concentrate ICP (AL-DS) as expressed in Eqs. (7) and (8), respectively [38,39].

$$J_v = \frac{D}{S}\left[\mathrm{Ln}\frac{A\pi_{draw} + B}{A\pi_{feed} + B + J_v}\right] \quad (7)$$

$$J_s = \frac{D}{S}\left[\mathrm{Ln}\frac{A\pi_{draw} + B - J_v}{A\pi_{feed} + B}\right] \quad (8)$$

In these two equations, D is the solute diffusion coefficient; π_{draw} and π_{feed} are the osmotic pressures of the draw solution and feed solution, respectively. So, the *S* value can be determined from these equations (Eqs. (7) and (8)).

4. FO Membrane Characterizations

Fourier transform infrared spectrometer (FTIR model: TENSOR 27, Germany) was used to evaluate the functional groups of PES support and TFN membranes. The XRD pattern of the PES-Fe_3O_4 substrates was examined at 2θ ranging from 10 to 80 using X-ray diffractometer (X' Pert Pro, Panalytical). Tensile mechanical properties of the PES and PES0.2 membranes were measured with an electronic strength tester (Gotech Universal AI-7000-LA, Taiwan) at a crosshead speed of 5 mm/min. At least four stripes were tested for each membrane to obtain the mean values of tensile stress and elongation at break of the membranes. Both top surface and cross-section morphologies of the PES and TFN membranes were examined using a field emission scanning electron microscope (FESEM: Mira 3-XMU). To evaluate the properties of voids (orientation and eccentricity), the data were extracted from FESEM images of the membrane cross section and were calculated using the image processing software. The orientation of voids is defined as the angle between a x-axis and a major axis of the fitting ellipse, and eccentricity is defined in terms of the minor and major axes of an ellipse [40]. For the cross section scanning, membrane samples were broken in liquid nitrogen. Then, all membranes were coated with a thin layer of gold to produce electric conductivity. Atomic force microscope (AFM model: Easyscan2 flex) was used to analyze the surface roughness and morphologies of the membranes. AFM with contact mode in the scale of 5 μm×5 μm was used in these experiments. A contact angle measuring instrument (Canon camera, Japan) was applied to evaluate membrane surface hydrophilicity. The contact angles reported are the averages of five random locations for each membrane to minimize the experimental error. Substrate porosity ε (%) was determined by measuring the wet mass (m_{wet}) and dry mass (m_{dry}) of membrane according to the following [41]:

$$\varepsilon = \frac{(m_{wet} - m_{dry})/\rho_w}{((m_{wet} - m_{dry})/\rho_w) + (m_{dry}/\rho_m)} \times 100 \quad (9)$$

where ρ_w and ρ_m are the density of water and membrane, respectively.

Guerout-Elford-Ferry equation (Eq. (10)) was used to calculate PES membrane mean pore radius (r_m) based on the water flux and porosity data [42-44].

$$r_m = \sqrt{\frac{(2.9-1.75\varepsilon)\times(8\eta l Q)}{\varepsilon \times A \times \Delta P}} \quad (10)$$

where η is the water viscosity (8.9×10^{-4} Pa·s), l is the PES membrane thickness (m) and Q is volume of permeate pure water per unit time (m^3/s).

RESULTS AND DISCUSSION

1. Effect of Fe_3O_4 Loadings on the Properties of PES Substrate

Table 2 presents the changes in the structural properties of PES substrate with and without impregnation of Fe_3O_4 NPs. Clearly, the pure water flux of the PES substrate was significantly improved when

Table 2. Effect of Fe_3O_4 concentration on the properties of PES substrate with respect to pure water permeability, contact angle, overall porosity and *S* value

Membranes	Pure water permeability (L/m^2 h bar)	Contact angle (°)	Overall porosity (%)	*S* value (mm)
PES (control)	120.4±8	71±2	80±1.9	0.78±0.06
PES 0.06	154.6±10	67±1.6	83.2±2.4	0.6±0.05
PES 0.1	185.4±13	65±1.5	85.5±2.2	0.53±0.05
PES 0.2	214.4±11	62±1.6	87±2.3	0.42±0.03
PES 0.3	174±9	60±1.3	85.3±1.8	0.53±0.01
PES 0.4	124.6±10	59±0.8	83.4±1.9	0.71±0.02
PES 0.5	102±7	58±1	81±1.4	0.85±0.06

[a]Pure water permeability of PES membrane was determined at operating pressure of 2.5 bar

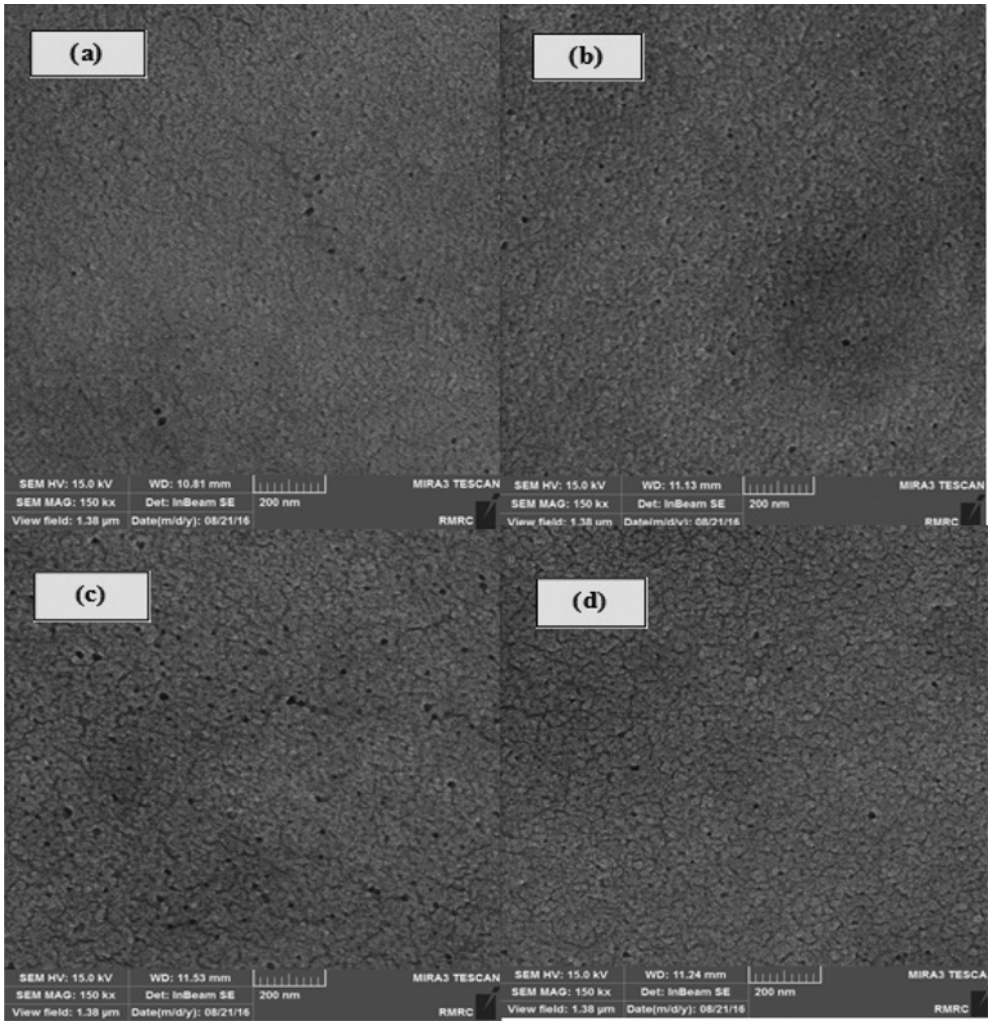

Fig. 1. FESEM of the top surface of PES substrates prepared from different nanoparticles loadings, (a) PES (control), (b) PES 0.1, (c) PES 0.2 and (d) PES 0.5.

only 0.2 wt% Fe_3O_4 NPs was used. The reasonable explanation is attributed to the increased membrane hydrophilicity and overall porosity. As shown in Table 2, the hydrophilicity of PES substrate was improved remarkably with the addition of hydrophilic Fe_3O_4 NPs into the casting solution. The reduction of water contact angle value from 71 °C to 58 °C in the PES substrate containing 0.5 wt% Fe_3O_4 NPs demonstrated the enhancement hydrophilicity of modified PES substrate.

The surface porosity of PES substrates prepared with various Fe_3O_4 NPs loading is shown in Fig. 1. Also, from the FESEM images,

Table 3. Effect of Fe_3O_4 concentration on the properties of PES substrate with respect to thickness, tortuosity/porosity, pore size, mean orientation and mean eccentricity

Membranes	Thickness (μm)	Tortuosity/ Porosity	Mean pore radius[a] (nm)	Mean pore radius[b] (nm)	Mean orientation (deg)	Mean eccentricity
PES (control)	139.9±2.6	5.59±0.11	1.9971	35.3	6.0002	0.17029
PES 0.1	104.88±2.1	5.05±0.14	2.1361	35.5	3.5872	0.2222
PES 0.2	99.47±1.5	4.22±0.1	2.2614	36.5	3.2389	0.22529
PES 0.5	80.55±1.2	0.55±0.02	2.1924	26.9	2.1002	0.21524

[a]The mean pore radius calculated by quantitive image computing
[b]The mean pore radius calculated by Eq. (10)

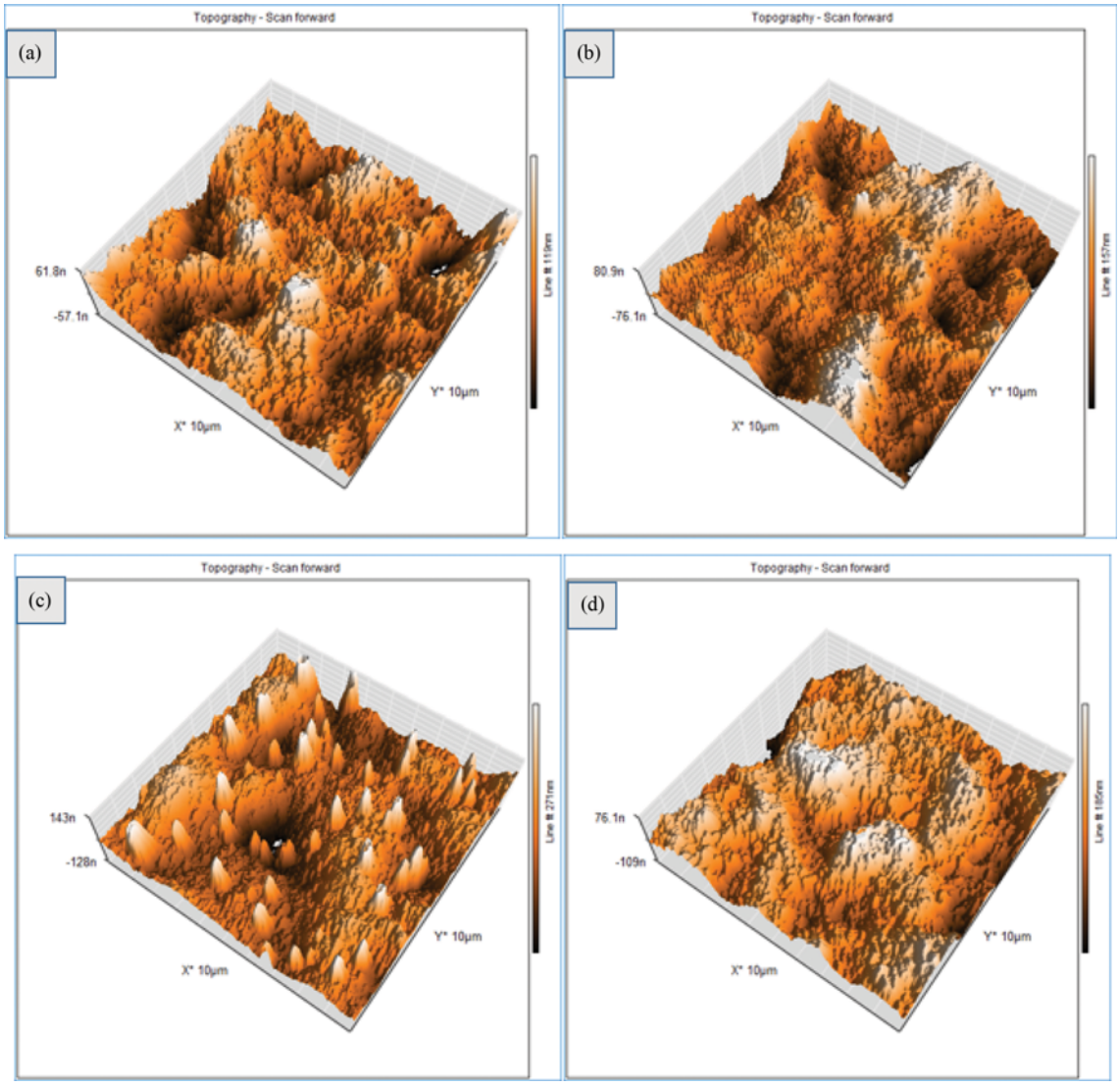

Fig. 2. AFM images of the top surface of PES substrates prepared from different Fe_3O_4 nanoparticles loadings, (a) PES (control), (b) PES0.1, (c) PES0.2 and (d) PES0.5.

the mean pore sizes were calculated by quantitive image computing [38] and summarized in Table 3. At low Fe_3O_4 content (≤0.2% w/w), increasing in Fe_3O_4 content improved porosity and the pore sizes which were mainly due to the diffusion of Fe_3O_4 NPs toward the coagulation bath during phase inversion.

At higher Fe_3O_4 content (≥0.3% w/w), on one hand, the exchange rate between solvent and nonsolvent was reduced due to a relatively high viscosity of the casting solution which was visually observed; on the other hand, a majority of Fe_3O_4 nanospheres could not diffuse into the coagulating bath before the solidification of support layer, and then had to be placed within the support structure or near the surface, It means that minor parts of Fe_3O_4 content contribute to complete the pore formation process [45-47]. Therefore, the surface porosity and the pore size of the support containg 0.5% w/w Fe_3O_4 was smaller than a support layer prepared using 0.2% w/w Fe_3O_4. Furthermore, a reduction in membrane pore size and porosity with increasing in loading of Fe_3O_4 could be ascribed to the pore blocking effect at the high concentration of Fe_3O_4 NPs and the remarkable agglomeration at high

Table 4. Effect of Fe_3O_4 loading on the surface roughness parameters of the PES substrates by AFM analysis

Membrane	Roughness		
	S_a (nm)	S_q (nm)	S_y (nm)
PES (control)	12.476	15.725	113.25
PES 0.1	34.476	45.045	342.42
PES 0.2	41.483	54.383	501.16
PES 0.5	36.723	51.75	496.11

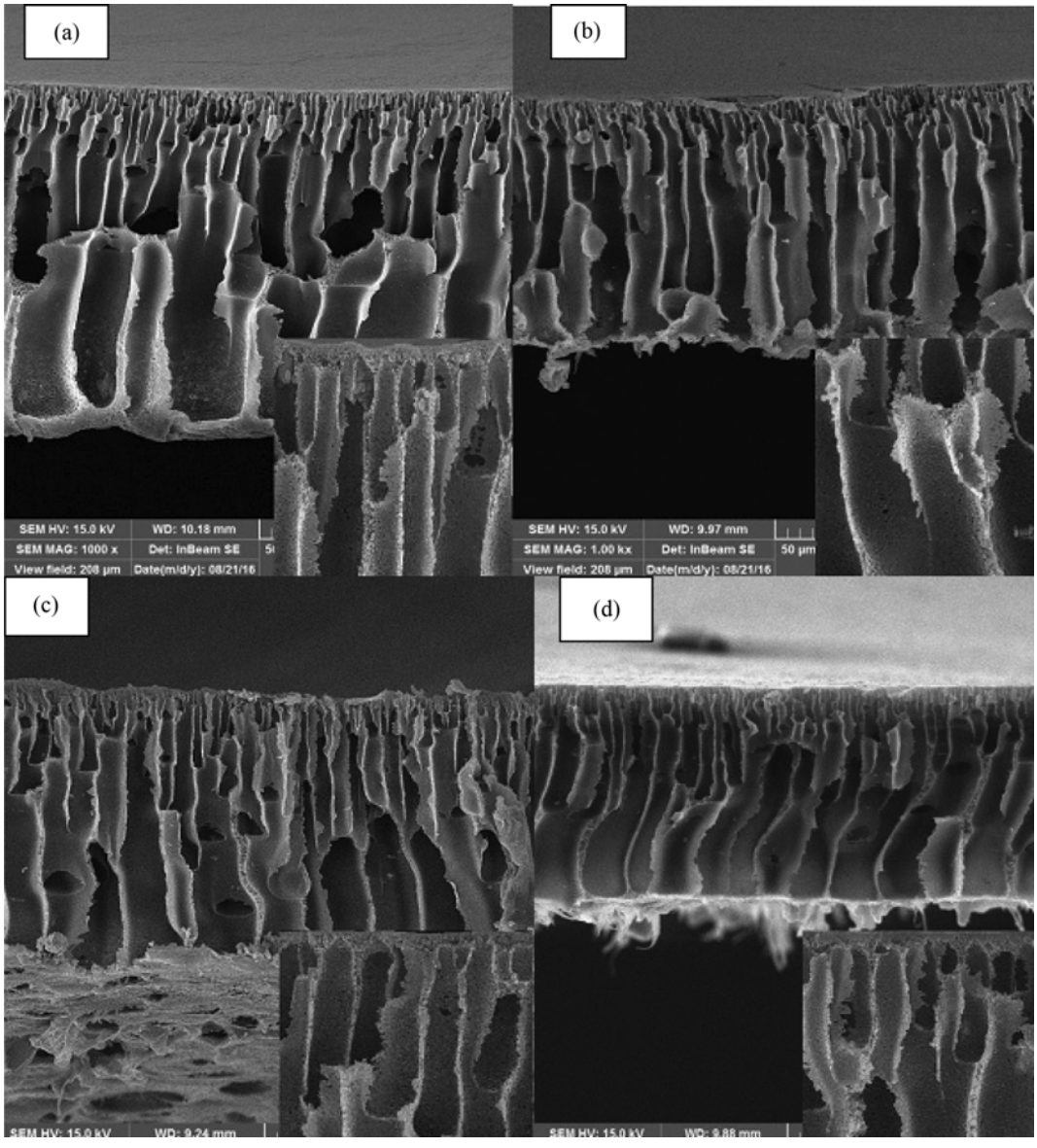

Fig. 3. FESEM of the cross section of PES substrates prepared from different nanoparticles loadings, (a) PES (control), (b) PES 0.1, (c) PES 0.2 and (d) PES 0.5.

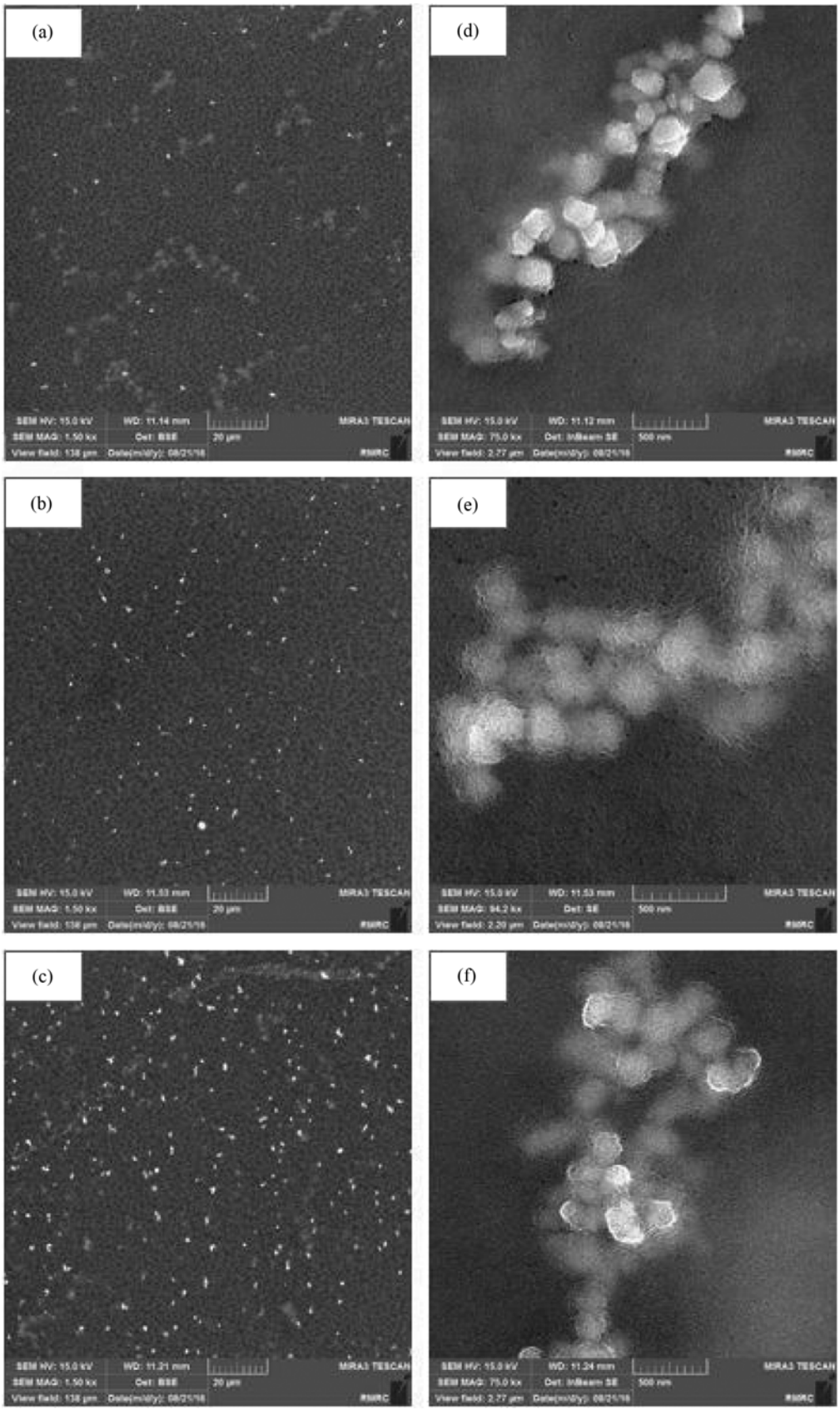

Fig. 4. FESEM of the top surface of PES prepared from different nanoparticles loadings, (a) PES0.1 at low magnification, (b) PES0.2 at low magnification, (c) PES0.5 at low magnification, (d) PES0.1 at high magnification, (e) PES0.2 at high magnification and (f) PES0.5 at high magnification.

Fe_3O_4/PES blending ratio. High magnification of FESEM images for substrate of TFC and TFN membrane shown in Fig. 4 confirms this observation clearly.

An increment in the overall porosity of substrate leads to a significant decline in mass transfer resistance and acts as the main contributor for smaller *S* value. In general, a smaller *S* value offers a better performance of the sublayer in reducing the effect of ICP phenomenon during the FO process [48]. Based on the data obtained, it is sensible to conclude that the increased water permeation of substrate at higher Fe_3O_4 loading is mainly due to the increment in substrate hydrophilicity coupled with increased porosity and pore sizes.

With respect to substrate surface roughness, Fe_3O_4 NPs played an important role in substrate surface roughness. Using the 3D AFM images, the changes in the PES membranes surface roughness are shown in Fig. 2, while the roughness parameters of membranes are summarized in Table 4 in terms of the average roughness (S_a), the squared root of mean the Z (S_q) and the mean height difference between the peaks and valleys (S_z). The observed increase in substrate surface roughness with an increase in Fe_3O_4 incorporation (≤0.2% w/w) is possibly ascribed to the amount of Fe_3O_4 NPs embedded in substrate matrix. The increase in water flux with the increase in roughness was ascribed to the increment of the area available for the water transport [49-51]. Further enhancment in Fe_3O_4 NPs demonstrated a negative impact on substrate surface roughness. This may be attributed to the decrease in pore size of membrane with high concentration of the Fe_3O_4 NPs.

Fig. 3 shows the cross section imgaes of PES substrates prepared with various Fe_3O_4 NPs incorporations. From the FESEM images, it can be seen that longer finger-like structures were extended from the top of the support layer to the bottom by adding Fe_3O_4 NPs into PES substrate. Also, the membrane eccentricity was estimated by calculating FESEM images. Eccentricity can be measurably considered as a function of finger-like structures or sponge-like structure. When membrane eccentricity is equal to 1, the membranes show macrovoids structure with a completely ellipse shape like finger-like structures and vice versa. At the present of Fe_3O_4 NPs, the membranes showed higher eccentricity than a neat membrane as shown in Table 3. The longer finger-like structure is favored for FO membranes because it produces less resistance to water and salt diffusion and consequently decreases the ICP propensity of membranes. The changes in sublayer morphology upon addition of Fe_3O_4 NPs could be attributed to the faster exchange rate between solvent (DMF) and nonsolvent (water) during the phase inversion process. In comparison with the pristine PES casting solution, transport of water from coagulation bath to the polymer film

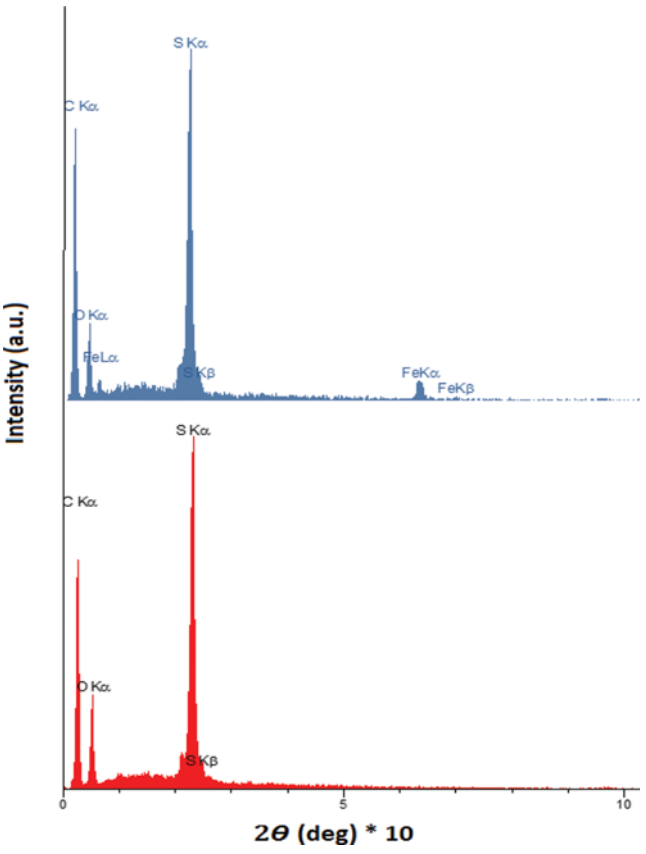

Fig. 5. EDX patterns for substrate (control) and substrate0.2.

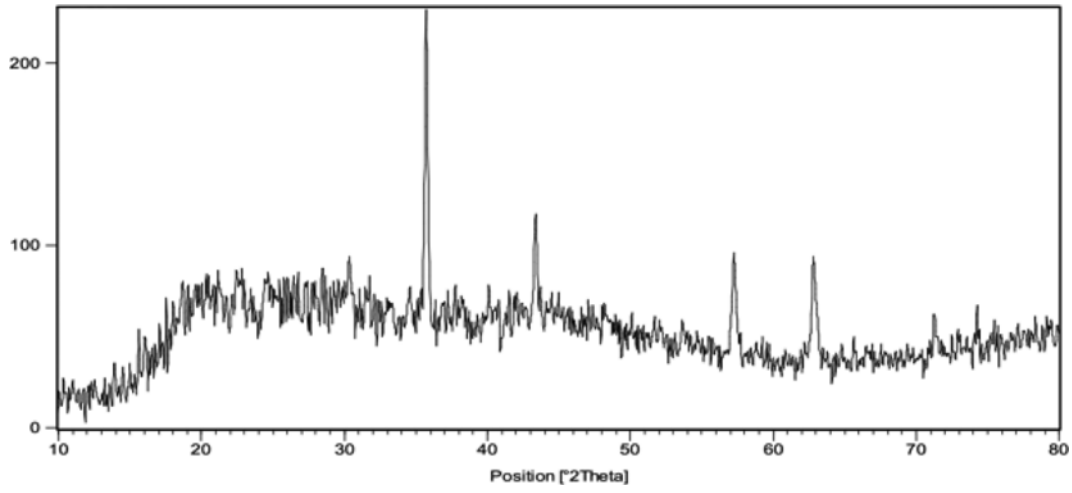

Fig. 6. XRD pattern of Fe_3O_4 nanoparticle in the PES substrate.

is facilitated with addition of hydrophilic Fe_3O_4 into the casting solution, resulting in long finger-like structure formation [21]. To evaluate the membrane orientation, the data were extracted from FESEM images of the membrane cross section using the image processing software. Table 3 presents the changes in the substrate orientation at different loadings of Fe_3O_4 NPs. The orientation of substrate was decreased when loading of Fe_3O_4 NPs was increased. It is obvious that decreasing substrate orientation is preferable for a substrate in order to minimize the ICP effect as a result of the increase of the area available for the water transport.

Fig. 4 shows the existence of Fe_3O_4 NPs on the top surface of the PES substrate. Clearly, more nanoparticle agglomeration (small white spots on FESEM images) took place on the top surface of sublayer as the Fe_3O_4 loading increased. The permanent attachment of these Fe_3O_4 NPs to the PES substrate matrix is a result of the combined effects of physical and chemical interactions [22]. Also, the presence of Fe_3O_4 NPs within the substrate matrix was confirmed by EDX results and XRD data as shown in Figs. 5 and 6, respectively. Fig. 6 shows the pattern of Fe_3O_4 crystal powders which has six crystalline characteristic peaks at 2θ of 30.0°, 35.3°, 42.9°, 53.5°, 57° and 62.4°, which are consistent with the values reported by Zhuang and et al. [52]. Table 5 summarizes the tensile strength and elongation at break of the PES and PES0.2 membranes. As shown, all the mechanical properties of PES0.2 membrane were better than PES membrane. It means that the loading of Fe_3O_4 nanoparticles increased the mechanical properties. This increase in mechanical properties of PES0.2 membrane can be attributed to the physical interaction between Fe_3O_4 nanoparticles and PES polymer. Fe_3O_4 could operate as a barrier in PES0.2 membrane to limit the chain mobility of PES and increase the strength of PES chain. So more energy is required to slide PES chains tied by Fe_3O_4 and the mechanical properties of PES membrane were improved [53].

Table 5. Mechanical properties of PES and PES0.2 membranes

Membranes	Tensile strengt (MPa)	Elongation at break (%)
PES	2.6±0.09	13.00±1.2
PES 0.2	3.12±0.1	25.83±2.1

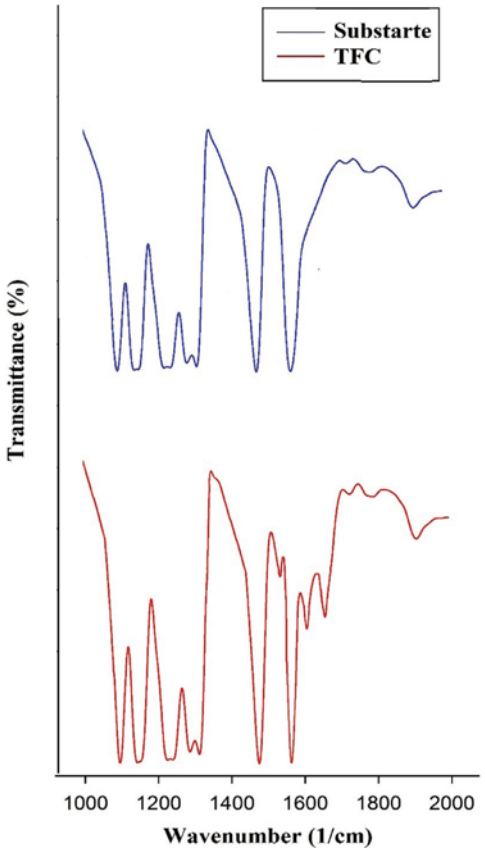

Fig. 7. ATR-FTIR spectra from 2,000 to 1,000 cm^{-1} for substrate (control) and TFC membrane.

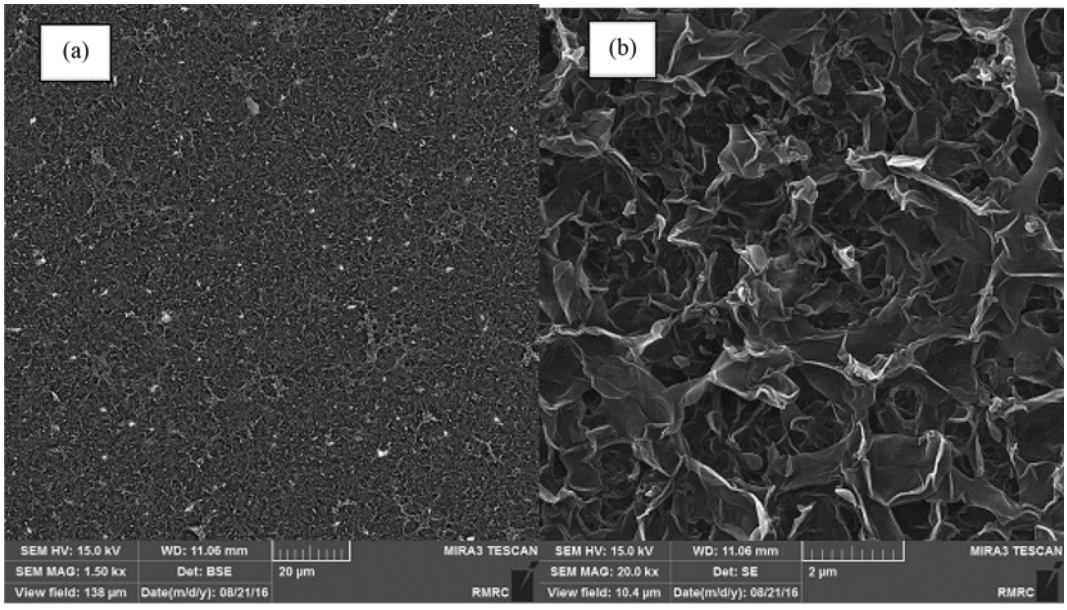

Fig. 8. FESEM of the top surface of the TFC membrane at (a) low magnification (b) high magnification.

2. TFN Membranes Prepared from PES and PES-Fe_3O_4 Substrate

Fig. 7 illustrates the ATR-FTIR spectra of PES support layer and TFC membrane prepared in this study. The peaks at the wave numbers of 1,104 cm^{-1} (C-O stretching vibration), 1,149 (O-H deformation and C-O stretching vibration interaction), 1,298 and 1,239 (C-O-C stretching vibrations), 1,484 (C-S), 1,322 (-SO_2- asymmetric stretching vibration) and 1,576 (aromatic systems) corresponded to the specific functional groups of PES support [54,55]. A comparison between the PES substrate spectrum and the TFC membrane spectrum, however, revealed the characterizing peaks of PA layer formed with MPD and TMC monomers at 1,662 cm^{-1}, 1,542 cm^{-1}, 1,612 cm^{-1}, which correspond to amide I band (C=O stretching), amide II band (C-H stretching) and aromatic ring breathing, respectively [55].

The rejection layer of TFC membrane was synthesized on the top of PES substrates by interfacial polymerization. Fig. 8(a) and (b) presents the top surfaces of the TFC membrane at both low and high magnifications, respectively. The TFC membrane shows a ridge-valley surface structure that is a typical morphology for polyamide membranes formed by MPD and TMC monomers [56,57].

3. Effect of Fe_3O_4 Loading on the Performance of TFN Membrane During RO Experiments

The effect of Fe_3O_4 loading on water permeability and NaCl rejection rate was evaluated using cross-flow RO tests and the results are shown in Fig. 9. At operating pressure of 2.5 bar, the TFC membrane tested with 20 mM NaCl aqueous solution demonstrated water permeability of 1.96 L/m^2 h bar and 96.3% NaCl rejection, while the TFN membrane containing 0.2 wt% Fe_3O_4 (TFN0.2) exhibited water permeability of 3.08 L/m^2 h bar, which was 57% higher than that of control TFC membrane. The improved water permeability of TFN membranes can be justified by the higher porosity and better hydrophilicity of the PES substrates also the subsequent formation of more open rejection layers and providing extra water pathways.

Further increasing Fe_3O_4 nanoparticles demonstrated a negative impact on membrane water permeability, which was reduced to 6.4 L/m^2 h bar, 4.95 L/m^2 h bar and 4.15 L/m^2 h bar, for TFN0.3, TFN0.4 and TFN0.5, respectively. The decreasing trend can be attributed to the pore blockage and a decrease in porosity of membrane at higher concentration of the Fe_3O_4 NPs. However, the TFN0.2 membrane exhibited 93.2% salt rejection, which was slightly lower compared to that of TFC control membrane. We believe that the reduction in NaCl rejection is owing to the lower degree of cross-linking formed in the active layer that is caused by the Fe_3O_4 agglomeration on PES substrate. Further increase in Fe_3O_4 loading enhanced NaCl rejection.

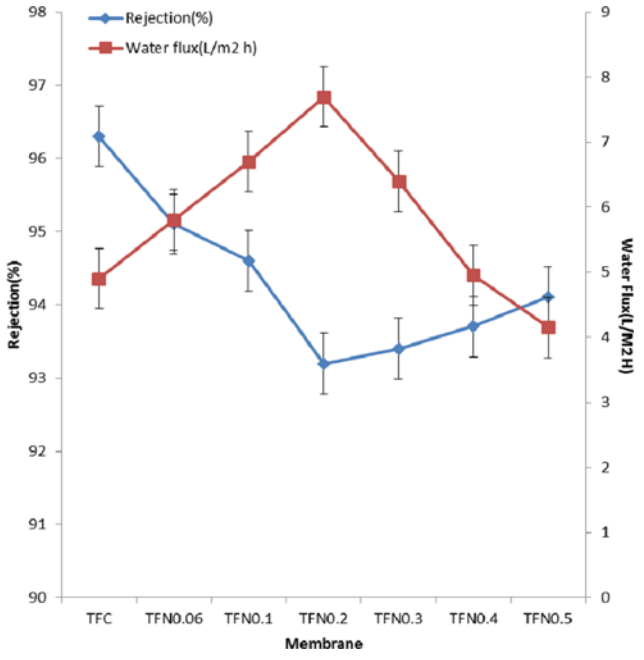

Fig. 9. Water flux and salt rejection of TFC/TFN membranes prepared from different types of PES substrates (Test conditions: 2.5 bar and 20 mM NaCl aqueous solution).

Table 6 compares the NaCl rejection and water permeability of membranes prepared in this work with two commercial cellulose triacetate (CTA) membranes): CTA-W and CTA-NW. With respect to pure water permeability, the PES substrate with Fe_3O_4 addition played a significant role in enhancing TFC membrane efficiency. All the synthesized TFN membranes showed much higher pure

Table 6. Comparison between the separation properties of TFC/TFN membranes prepared in this work and commercial CTA membranes

Membranes	Water permeability (L/m^2 h bar)[a]	Water permeability A ($\times10^{-12}$ m/s Pa)[a]	Salt permeability B ($\times10^{-8}$ m/s)[b]	B/A (kPa)	References
TFC (control)	1.96±0.21	5.44±0.3	5.23±1.4	9.61±3	In this work
TFN 0.06	2.32±0.23	6.44±0.4	8.3±1.6	12.9±3	In this work
TFN 0.1	2.68±0.26	7.44±0.5	10.62±1.7	14.27±4	In this work
TFN 0.2	3.08±0.27	8.55±0.5	15.60±1.8	18.24±5	In this work
TFN 0.3	2.56±0.24	7.11±0.5	12.56±1.8	17.66±4	In this work
TFC 0.4	1.98±0.2	5.5±0.4	9.24±1.5	16.8±6	In this work
TFN0.5	1.66±0.18	4.61±0.3	7.23±1.5	15.6±5	In this work
CTA-W	0.33±0.04	0.9±0.1	4±0.9	47±12	[10]
CTA-NW	0.46±0.07	1.3±0.2	2.7±0.2	22±3	[10]

[a]Water permeabilities were measured in RO testing mode at 2.5 bar pressure and DI water as feed solution
[b]Salt permeabilities were measured in RO testing mode at 2.5 bar pressure and 20 mM NaCl as feed solution

water permeability than those of commercial CTA membranes. As the polyamide active layer of the composite membrane is very thin, the transport resistance of water molecules is to be minimal in comparison to the commercial CTA membranes. Because of this fact, the water permeability achieved by the TFN0.2 membrane was close to 9.3-times and 6.7-times higher than the CTA-W and CTA-NW membranes, respectively. With respect to salt permeability/pure water permeability (B/A) ratio, all of the in-house-made composite membranes displayed smaller values compared to the commercial membranes. The smaller value of B/A ratio showed more efficiency for our in-house membranes in decreasing solute reverse flux during FO process [10].

4. Effect of Fe_3O_4 Loading on the Performance of TFC/TFN Membrane During FO Test

4-1. Results for 10 mM NaCl as Feed Solution

Fig. 10 presents the water flux of TFC membranes evaluated by

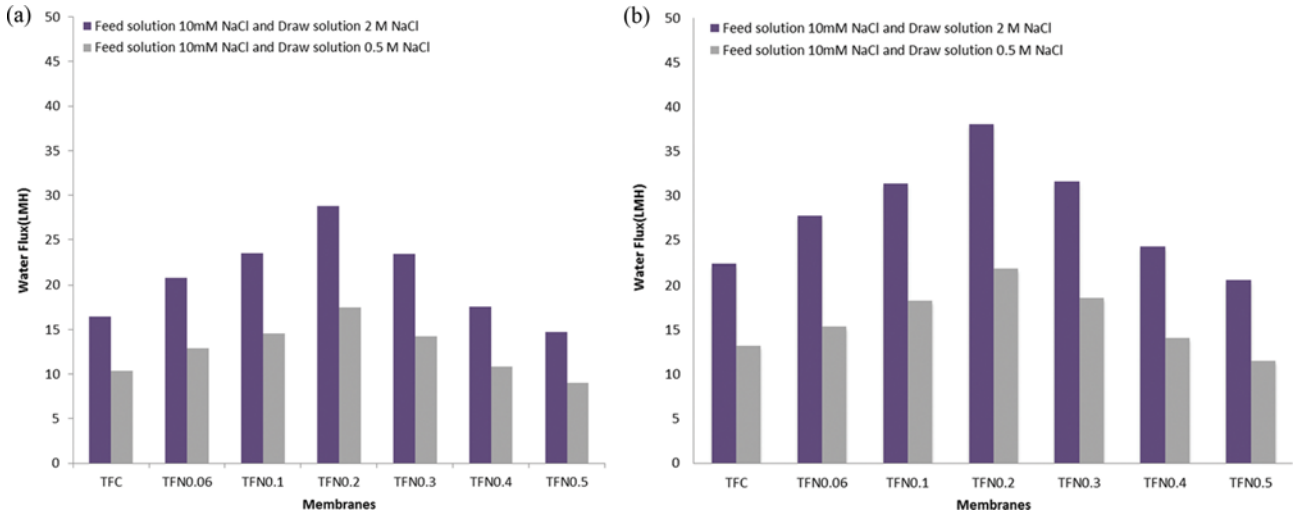

Fig. 10. Water flux of FO membrane prepared from PES substrate made of different Fe_3O_4 loading, (a) AL-FS orientation and (b) AL-DS orientation.

Table 7. Comparison between the performance of the TFC/TFN FO membranes prepared in this work and TFC/TFN FO membranes reported in the literature

Membranes	Water flux (L/ m^2 h) FO/PRO	Reverse salt flux (g/m^2 h) FO/PRO	Feed solution	Draw solution	References
TFC (control)	10.4±0.5/13.2±0.6	2.1±0.1/4.1±0.3	10 mM NaCl	0.5 M NaCl	In this work
	16.5±0.7/22.4±0.8	5.9±0.3/10.1±0.5	10 mM NaCl	2 M NaCl	In this work
TFN 0.06	12.9±0.5/15.4±0.6	2.9±0.1/5.4±0.3	10 mM NaCl	0.5 M NaCl	In this work
	20.78±0.7/27.77±0.9	8.5±0.4/13.2±0.6	10 mM NaCl	2 M NaCl	In this work
TFN 0.1	14.6±0.6/18.3±0.7	3.5±0.1/6.3±0.3	10 mM NaCl	0.5 M NaCl	In this work
	23.52±0.8/31.4±1	11.6±0.5/16.8±0.6	10 mM NaCl	2 M NaCl	In this work
TFN 0.2	17.5±0.7/21.9±0.8	4.9±0.5/7.9±0.5	10 mM NaCl	0.5 M NaCl	In this work
	28.8±0.9/38.08±1.2	14.7±0.7/20.1±0.9	10 mM NaCl	2 M NaCl	In this work
TFN 0.3	14.21±0.6/18.6±0.7	4.1±0.4/7.1±0.6	10 mM NaCl	0.5 M NaCl	In this work
	23.42±0.8/31.6±1	12.2±0.7/17.3±0.8	10 mM NaCl	2 M NaCl	In this work
TFC 0.4	10.8±0.5/14.1±0.6	3.6±0.2/6.4±0.4	10 mM NaCl	0.5 M NaCl	In this work
	17.56±0.7/24.33±0.9	10.4±0.5/15.9±0.7	10 mM NaCl	2 M NaCl	In this work
TFN 0.5	9±0.4/11.5±0.5	2.7±0.1/5.2±0.3	10 mM NaCl	0.5 M NaCl	In this work
	14.75±0.6/20.6±0.6	8.1±0.4/12.8±0.5	10 mM NaCl	2 M NaCl	In this work
CTA-W	5.00/6.55	5.3/4.8	10 mM NaCl	0.5 M NaCl	[10]
	12.1/22.9		10 mM NaCl	2 M NaCl	[10]
CTA-NW	4.42/8.19	2.9/2.8	10 mM NaCl	0.5 M NaCl	[10]
	8.54/21.8		10 mM NaCl	2 M NaCl	[10]
CNF-NH_2	18/-	0.5	10 mM NaCl	1 M NaCl	[35]
TFC 21	17/27.6	-	DI water	2 M NaCl	[28]
TFC-FO	21/33	2.2/2.8	DI water	2 M NaCl	[2]
TFN 0.05	22.5/36.5	-	10 mM.NaCl	2 M NaCl	[60]

the cross-flow FO process at AL-FS and AL-DS orientations. The experiments were performed using either 0.5 M NaCl or 2 M NaCl as draw solution and 10 mM NaCl as feed solution. Results showed that the TFN membranes prepared from PES-Fe_3O_4 substrates showed much higher water flux for both draw solutions compared to the control TFC membrane. However, the addition of more than 0.2 wt% of the Fe_3O_4 NPs results in lower water flux which can be attributed to pore blockage. Based on the results obtained from the RO and FO experiments, it is concluded that Fe_3O_4 NPs loading of 0.2 wt% was the optimal loading for PES-Fe_3O_4 sublayer preparation to produce a promising performance for TFN membrane resulting in high water flux and porosity. Fig. 10 illustrates that by adding only 0.2 wt% Fe_3O_4, the water flux increased from 10.4 L/m^2 h of TFC (control) to 17.5 L/m^2 h of TFN0.2 in AL-FS (for 0.5 M NaCl as draw solution) and from 13.2 L/m^2 h of TFC (control) to 21.9 L/m^2 h of TFN0.2 in AL–DS (for 0.5 M NaCl as draw solution). Results in Table 7 and Fig. 10 show the same trend, but the membranes evaluated at AL-DS orientation have exhibited notably higher water flux. The decrease in osmotic pressure differential owing to ICP phenomenon can be considered as the major reason for the lower water flux in AL-FS orientation [58]. A similar increasing trend was also observed when 2 M NaCl draw solution was replaced with 0.5 M NaCl solution, but with a much greater water flux produced. This is due to the increase of osmotic pressure difference that noticeably improves the driving force and the water flux of the FO penetration process. However, the increment of water flux is not as much osmotic pressure difference increment, because the osmotic pressure loss across the membrane increases accordingly as the draw solution concentration enhancement. This incompatibility may attribute to the deterioration of dilutive ICP [6].

It has been proven that modifying PES support layer properties by adding Fe_3O_4 NPs could also be an effective way to enhance FO performance of typical thin film composite membrane. One of the main factors that reduce ICP during FO process is the *S* value. Since the effect of ICP on FO process can be minimized by reducing *S* value, it seems that modification of the PES substrate through loading of Fe_3O_4 NPs is an acceptable strategy to improve the TFC membrane efficiency in FO process. Also, Fe_3O_4 NPs have significantly increased the mass transfer efficiency of PES substrate where the *S* value of substrate (0.2) was much smaller (0.42 mm) compared to that of PES substrate (0.78 mm). These findings agree with the substrate characterization discussed earlier (Section 3.1) that a substrate containing 0.2 Fe_3O_4 NPs has shown higher hydrophilicity, higher overall porosity, and lower thickness compared to pristine PES. Given the fact that tortuosity/porosity ratio straightly influences the *S* value, it is logical to witness a reduction in *S* parameter for substrate. As can be seen in Table 3, by increasing Fe_3O_4 NPs the tortuosity/porosity ratio decreases and leads to reducing the ICP propensity of membranes. Also, reports show that substrates with higher hydrophilicity are more favorable for reducing ICP phenomenon [20]. Furthermore, Fe_3O_4 incorporation in the support layer facilitates water transport as it provides extra water pathways in the support layer. This improved pure water flux (as shown in Table 2) and consequently increased mass transfer coefficient of the support layer. The results obtained in this study offer that addition of Fe_3O_4 to the PES support layer improves FO pure water flux performance through (1) increasing the water permeability of the active layer, and (2) minimizing the ICP phenomenon inside the support layer by reducing the *S* value.

The NaCl salt fluxes of membranes tested in both AL-FS and AL-DS modes are shown in Fig. 11. The trend of NaCl salt flux was well correlated to the trend of NaCl salt rejection data in RO shown in Fig. 9, where a high rejection rate corresponds to a low solute flux and vice versa. A high level of solute flux must be avoided insofar as it would result in remarkable ICP and membrane fouling problem during FO test [59]. Despite the significant enhancement in water flux achieved by TFN0.2 membranes, there were insignificant differences in terms of NaCl salt flux of TFN0.2 membrane compared to TFC membranes fabricated with PES only. Further increasing in Fe_3O_4 NPs loading up to 0.3 wt% reduced the NaCl solute flux.

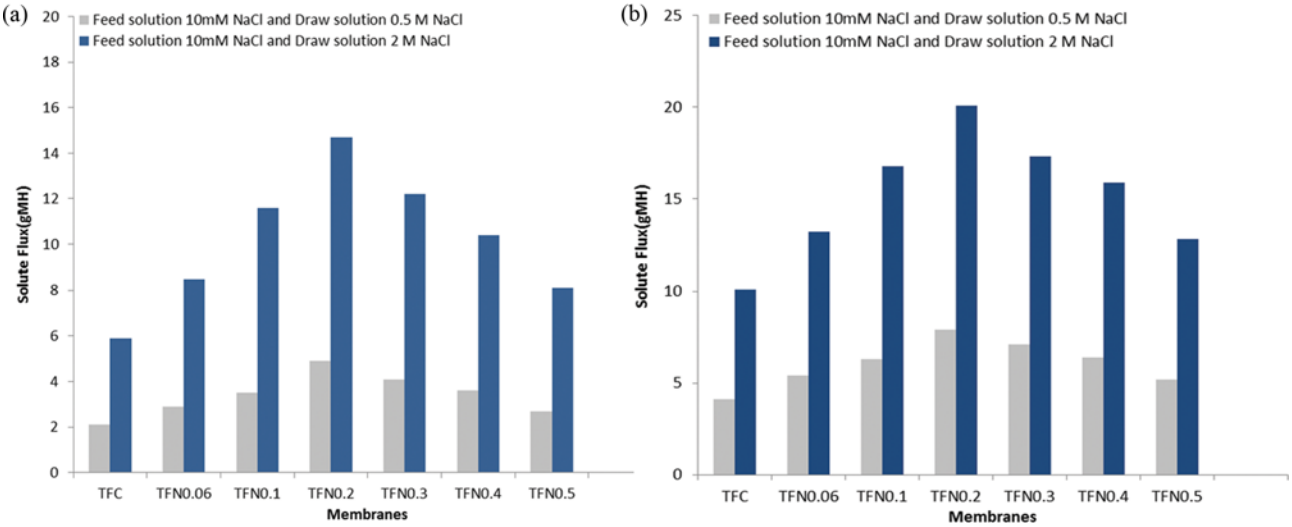

Fig. 11. Solute flux of FO membrane prepared from PES substrate made of different Fe_3O_4 loading, (a) AL-FS orientation and (b) AL-DS orientation.

Table 7 compares the water flux and salt flux of the TFC/TFN membranes with two commercial CTA membranes. All the TFC/TFN membranes showed much higher water flux than those of commercial CTA membranes. The better water flux and lower salt flux of our in-house membranes can be attributed to the higher porosity and lower *S* value [10] of our TFC/TFN membranes. The current study suggests that TFC membranes offer remarkable advantages over CTA membranes because (1) the TFC way allows flexibility for autonomous optimization of the support layer and the polyamide layer, and (2) the polyamide layer formed with interfacial polymerization also tends to have better water flux and solute rejection [10].

Along with comparison to commercial CTA membranes, the TFN0.2 membrane was also compared to other FO membranes reported in the literature. As shown in Table 7, our TFN0.2 membranes exhibit better water flux than FO membranes reported in the literature [2,27,35,60].

4-2. Results for Caspian Seawater as Feed Solution

FO is a most promising process for seawater desalination, so in this section Caspian seawater was applied to evaluate the performance of TFC and TFN membranes. The performance was evaluated with Caspian seawater as feed solution and 2 M NaCl as draw solution in both AL-FS and AL-DS modes. Fig. 12 and Table 8 illustrate that by adding only 0.2 wt% Fe_3O_4, the water flux increased from 7.2 L/m^2 h in the TFC membrane to 12.3 L/m^2 h in the TFN0.2 membrane (i.e., ~70% increase) and from 9.6 L/m^2 h to 16.6 L/m^2 h (i.e., ~73% increase) for AL-FS and AL-DS orientations, respectively. Comparing Fig. 12 with Fig. 10 shows that the water flux of TFC and TFN membranes decreased significantly for seawater concentration. The results can be explained as follows: when seawater or a certain concentration of feed solution was taken instead of the 10 mM NaCl, a concentrative ECP emerged on the membrane active layer side, and the high draw solution concentration also led to a more serious dilutive ICP on membrane support layer. As a result, the severe CPs on both sides of the membrane raised the osmotic pressure drop through the membrane and consequently lowered the water fluxes. However, the water flux of TFN0.20 membrane was still higher than the TFC and all other TFN membranes in both AL-FS and AL-DS orientations due to the smaller *S* parameter of the sublayer and less severe ICP. It is noted that the component and concentration of feed solution could influence the selection of FO membrane orientation.

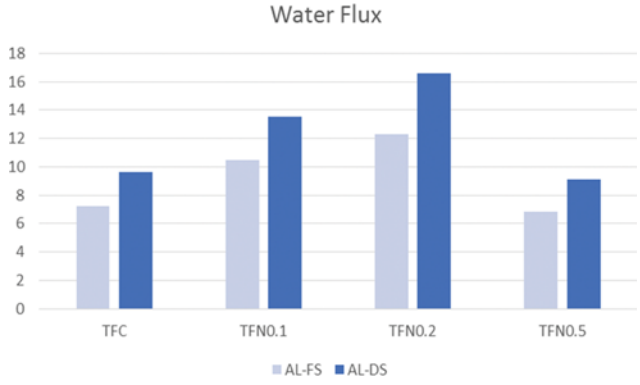

Fig. 12. Water flux of FO membranes in both AL-FS and AL-DS orientation using Caspian seawater as feed and 2 M NaCl as draw solution.

CONCLUSIONS

The properties of PES substrates for TFN FO membranes were successfully improved by loading different amounts of Fe_3O_4 NPs ranging from zero to 0.5 wt% into the substrate matrix. The results demonstrated that the porosity and the hydrophilicity of PES-Fe_3O_4 substrate have been successfully improved upon addition of Fe_3O_4 NPs. In RO tests, the water permeability of TFC membrane increased with addition of Fe_3O_4 incorporation, while salt rejection reduced slowly first, due to the defects of PA selective layer and increase slowly at Fe_3O_4 loading of ≥0.3 wt%, due to the pore blockage membrane during RO experimental. With respect to the FO tests, the TFC membrane prepared from PES substrate embedded with 0.2 wt% Fe_3O_4 exhibited the best performance in both AL-FS and AL-DS mods and for both low (0.5 M NaCl) and high (2 M NaCl) draw solution concentrations. This should be ascribed to the much smaller S value (S=0.42 mm) of TFN0.2 membrane that is supposed to play the main role in minimizing the effect of ICP phenomenon during the FO process. Facilitation of water transportation via formation of additional water pathways, higher hydrophilicity and improved overall porosity can be considered as the major factors behind reduction in *S* value. As a conclusion, this present work provides an insight that instead of modifying the properties of PA layer, improving the properties of the support layer, e.g. its porosity and hydrophilicity, could open up a new opportunity to improve FO membrane efficiency.

Table 8. Result for Caspian Seawater as feed solution

Membranes	Water permeability (L/m^2 h bar)[a]	Water permeability A ($\times10^{-12}$ m/s Pa)[a]	Salt permeability B ($\times10^{-8}$ m/s)[a]	*S* value (mm)	Water flux (L/m^2h)[b] FO	Water flux (L/m^2 h)[c] PRO
TFC (control)	1.09+0.12	3.03+0.21	2.18+0.4	1.94+0.11	7.2+0.33	9.6+0.45
TFC 0.1	1.41+0.15	3.91+0.28	4.83+0.9	1.27+0.09	10.5+0.45	13.5+0.52
TFC 0.2	1.76+0.16	4.88+0.31	7.8+1.4	1.11+0.08	12.3+0.51	16.6+0.6
TFC 0.5	0.98+0.08	2.72+0.23	3.66+0.5	2.01+0.11	6.8+0.31	9.1+0.32

[a]Water permeabilities were measured in RO testing mode at 2.5 bar pressure and Caspian Seawater as feed solution
[b]Water fluxes were measured in FO testing mode at Caspian Seawater as feed solution and 2 M NaCl as draw solution
[c]Water fluxes were measured in PRO testing mode at Caspian Seawater as feed solution and 2 M NaCl as draw solution

REFERENCES

1. T. Beyki and M. J. Asadollahzadeh, *J. Water Environ. Nanotechnol.*, **1**, 19 (2016).
2. N. Niksefat, M. Jahanshahi and A. Rahimpour, *Desalination*, **343**, 140 (2014).
3. N. Ma, J. Wei, R. Liao and C. Tang, *J. Membr. Sci.*, **405**, 149 (2012).
4. Ch. Bae, K. Park, H. Heo and D. R. Yang, *Korean J. Chem. Eng.*, **10**, 1975 (2016).
5. B. Khorshidi, A. Bhinder, T. Thundat, D. Pernitsky and M. Sadrzadeh, *J. Membr. Sci.*, **511**, 29 (2016).
6. Y. Wang, M. Zhang, Y. Liu, Q. Xiao and S. Xu, *Desalination*, **398**, 106 (2016).
7. T. Takahashi, M. Yasukawa and H. Matsuyama, *J. Membr. Sci.*, **514**, 547 (2016).
8. T. Ruprakobkit, L. Ruprakobkit and Ch. Ratanatamskul, *Chem. Eng. J.*, **306**, 538 (2016).
9. N. C. Nguyen, Sh. Chen, Y. Weng, H. Nguyen, S. S. Ray, Ch. Li, B. Yan and J. Wang, *J. Membr. Sci.*, **520**, 214 (2016).
10. J. Wei, Ch. Qiu, Ch. Y. Tang, R. Wang and A. G. Fane, *J. Membr. Sci.*, **372**, 292 (2011).
11. N. Akther, A. Sodiq, A. Giwa, S. Daer, H. A. Arafat and S. W. Hasan, *Chem. Eng. J.*, **281**, 502 (2015).
12. Y. Gao, Y. Wang, W. Li and Ch. Y. Tang, *Desalination*, **338**, 65 (2014).
13. Kh. Touati and F. Tadeo, *Desalination*, **389**, 171 (2016).
14. D. Y. Kim, B. Gu and D. R. Yang, *Korean J. Chem. Eng.*, **30**, 1691 (2013).
15. J. Gai and X. Gong, *J. Mater. Chem. A*, **2**, 425 (2014).
16. J. Li, Q. Liu, X. Li, Y. Liu and J. Xie, *Ind. Eng. Chem. Res.*, **55**, 5327 (2016).
17. D. L. Shaffer, J. R. Werber, H. Jaramillo, Sh. Lin and M. Elimelech, *Desalination*, **356**, 271 (2014).
18. M. Yasukawa, Sh. Mishima, M. Shibuya, D. Saeki, T. Takahashi, T. Miyoshi and H. Matsuyama, *J. Membr. Sci.*, **487**, 51 (2015).
19. J. M. Puguan, H. Kim, K. Lee and H. Kim, *Desalination*, **336**, 24 (2014).
20. D. Emadzadeh, W. J. Lau, T. Matsuura, M. Rahbari-Sisakht and A. F. Ismail, *Chem. Eng. J.*, **237**, 70 (2014).
21. D. Emadzadeh, W. J. Lau and A. F. Ismail, *Desalination*, **330**, 90 (2013).
22. M. Tian, Y. Wang, R. Wang and A. G. Fane, *Desalination*, **401**, 142 (2017).
23. J. Yin and B. Deng, *J. Membr. Sci.*, **479**, 256 (2015).
24. P. Goh and A. F. Ismail, *J. Chem. Technol. Biotechnol.*, **90**, 971 (2015).
25. L. Peng, L. Shuai, Z. Tuantuan, M. Xueyi, Z. Yu, Z. Cheng, U. Ahmad, W. Hongjie and W. Qiang, *Nanosci. Nanotechnol. Lett.*, **8**, 906 (2016).
26. M. Ghanbari, D. Emadzadeh, W. J. Lau, H. Riazi, D. Almasi and A. F. Ismail, *Desalination*, **377**, 152 (2016).
27. P. Lu, Sh. Liang, L. Qiu, Y. Gao and Q. Wang, *J. Membr. Sci.*, **504**, 196 (2016).
28. Zh. Liu, H. Yu, G. Kang, X. Jie, Y. Jin and Y. Cao, *J. Membr. Sci.*, **497**, 485 (2016).
29. F. Chen, Sh. Xie, X. Huang and X. Qiu, *J. Hazard. Mater.*, **322**, 152 (2016).
30. R. Davarnejad and P. Panahi, *Sep. Purif. Technol.*, **158**, 286 (2016).
31. S. Zinadini, A. A. Zinatizadeh, M. Rahimi, V. Vatanpour, H. Zangeneh and M. Beygzadeh, *Desalination*, **349**, 145 (2014).
32. A. Gholami, A. R. Moghadassi, S. M. Hosseini, S. Shabani and F. Gholami, *J. Ind. Eng. Chem.*, **20**, 1517 (2013).
33. J. Yang, P. Zou, L. Yang, J. Cao, Y. Sun, D. Han, Sh. Yang, Z. Wang, G. Chen, B. Wang and X. Kong, *Appl. Surf. Sci.*, **303**, 425 (2014).
34. S. Zhang, K. Y. Wang, T. Chung, H. Chen, Y. C. Jean and G. Amy, *J. Membr. Sci.*, **360**, 522 (2010).
35. Z. Dabaghian, A. Rahimpour and M. Jahanshahi, *Desalination*, **381**, 117 (2016).
36. M. Aminia, A. Rahimpour and M. Jahanshahi, *Desalination and Water Treatment*, 1 (2015).
37. S. Loeb, L. Titelman, E. Korngold and J. Freiman, *J. Membr. Sci.*, **129**, 243 (1997).
38. Z. Zhou, J. Y. Lee and T. Chung, *Chem. Eng. J.*, **249**, 236 (2014).
39. G. Mehta and S. Loeb, *J. Membr. Sci.*, **4**, 261 (1978).
40. P. Pouresmaeel-Selkjani, M. Jahanshahi and M. Peyravi, *High Performance Polymers*, 1 (2016).
41. J. Wei, Y. Li, L. Setiawan and R. Wang, *J. Membr. Sci.*, **511**, 54 (2016).
42. H. Yu, X. Zhang, Y. Zhang, J. Liu and H. Zhang, *Desalination*, **326**, 69 (2013).
43. S. Zinadini, A. A. Zinatizadeh, M. Rahimi, V. Vatanpour and H. Zangeneh, *J. Membr. Sci.*, **453**, 292 (2014).
44. E. Yuliwati, A. F. Ismail, T. Matsuura, M. A. Kassim and M. S. Abdullah, *Desalination*, **283**, 206 (2011).
45. H. Wu, B. Tang and P. Wu, *J. Membr. Sci.*, **451**, 94 (2014).
46. J. Shen, H. Ruan, L. Wu and C. Gao, *Chem. Eng. J.*, **168**, 1272 (2011).
47. S. Zinadini, A. A. Zinatizadeh, M. Rahimi, V. Vatanpour and H. Zangeneh, *J. Membr. Sci.*, **453**, 292 (2014).
48. Y. Wu, H. Zhu, L. Feng, L. Zhang and Sh. Xing, *Desalination and Water Treatment*, 1944 (2015).
49. M. Peyravi, A. Rahimpour, M. Jahanshahi, A. Javadi and A. Shockravi, *Micropor. Mesopor. Mater.*, **160**, 114 (2012).
50. M. Peyravi, M. Jahanshahi, A. Rahimpour, A. Javadi and S. Hajavi, *Chem. Eng. J.*, **241**, 155 (2014).
51. A. Mollahosseini, A. Rahimpour, M. Jahamshahi, M. Peyravi and M. Khavarpour, *Desalination*, **306**, 41 (2012).
52. L. Zhuang, W. Zhang, Y. Zhao, H. Shen, H. Lin and J. Liang, *Scientific Reports*, **5**, 9320 (2015).
53. Z. Huang, F. Zheng, Z. Zhang, H. Xu and K. Zhou, *Desalination*, **292**, 64 (2012).
54. E. Antón, J. R. Álvarez, L. Palacio, P. Prádanos, A. Hernández, A. Pihlajamäki and S. Luque, *Chem. Eng. Sci.*, **134**, 178 (2015).
55. S. H. Maruf, A. R. Greenberg and Y. Ding, *J. Membr. Sci.*, **512**, 50 (2016).
56. R. J. Petersen, *J. Membr. Sci.*, **83**, 81 (1993).
57. C. T ang, Q. Shiangfu, C. Criddle and A. Leckie, *Environ. Sci. Technol.*, **41**, 2008 (2007).
58. M. Xie, W. E. Price and L. D. Nghiem, *Sep. Purif. Technol.*, **93**, 107 (2012).
59. Sh. Zou, Y. Gu, D. Xiao and Ch. Y. Tang, *J. Membr. Sci.*, **366**, 356 (2011).
60. N. Widjojo, T. Chung, M. Weber, Ch. Maletzko and V. Warzelhan, *J. Membr. Sci.*, **383**, 214 (2011).